Pure Appl. Chem., Vol. 82, No. 11, pp. 2055–2073, 2010. doi:10.1351/PAC-CON-09-12-05 © 2010 IUPAC, Publication date (Web): 6 August 2010

Surface effects on optical and electrical properties of ZnO nanostructures*

Cheng-Ying Chen, Ming-Wei Chen, Jr-Jian Ke, Chin-An Lin, José R. D. Retamal, and Jr-Hau He[‡]

Institute of Photonics and Optoelectronics and Department of Electrical Engineering, National Taiwan University, Taipei 10617, Taiwan

Abstract: This article presents a comprehensive review of the current research addressing the surface effects on physical properties and potential applications of nanostructured ZnO. Studies illustrating the transport, photoluminescence (PL), and photoconductivity properties of ZnO with ultrahigh surface-to-volume (S/V) ratio are reviewed first. Secondly, we examine recent studies of the applications of nanostructured ZnO employing the surface effect on gas/chemical sensing, relying on a change of conductivity via electron trapping and detrapping process at the surfaces of nanostructures. Finally, we comprehensively review the photovoltaic (PV) application of ZnO nanostructures. The ultrahigh S/V ratios of nanostructured devices suggest that studies on the synthesis and PV properties of various nanostructured ZnO for dye-sensitized solar cells (DSSCs) offer great potential for high efficiency and low-cost solar cell solutions. After surveying the current literature on the surface effects on nanostructured ZnO, we conclude this review with personal perspectives on a few surface-related issues that remain to be addressed before nanostructured ZnO devices can reach their ultimate potential as a new class of industrial applications.

Keywords: electrical properties; nanostructures; nanowires; optical properties; surface effects; ZnO.

INTRODUCTION

The synthesis of a unique group of nanostructures of wurtzite ZnO is possible because of three types and a total of 13 fastest directions of growth (<0001>, $<01\bar{1}0>$, and $<2\bar{1}\bar{1}0>$), together with a pair of polar surfaces (0001). This group of nanostructures is exemplified by nanowires/nanorods (NWs/NRs) [1], nanoparticles (NPs) [2], 3D nanoarchitectures [3], nanojunction-arrays [4], nanobelts (NBs) [5], nanosprings [6], nanorings [7], and NR networks [8]. Moreover, nanostructured ZnO has attracted intensive research efforts for its versatile applications such as photodiodes [9,10], field-effect transistors (FETs) [11–13], light-emitting diodes (LEDs) [14], gas sensors [15,16], photodetecters [17–19], optical switches [18], second harmonics generators [20], solar cells [21,22], and thermal switches [23].

The surface effects—including surface band bending [24], chemisorption/photodesorption near surfaces [25,26], native surface defects/states [27], and surface roughness [13]—are more pronounced in the nanostructures than that in thin film and bulk counterparts due to the structural uniqueness and the ultrahigh surface-to-volume (S/V) ratio of ZnO nanostructures. In order to develop the novel appli-

^{*}Paper based on a presentation at the 5th International Symposium on Novel Materials and Their Synthesis (NMS-V) and the 19th International Symposium on Fine Chemistry and Functional Polymers (FCFP-XIX), 18–22 October 2009, Shanghai, China. Other presentations are published in this issue, pp. 1975–2229.

[‡]Corresponding author: E-mail: jhhe@cc.ee.ntu.edu.tw

cation of ZnO nanostructures utilizing the surface effect, it is very important to understand how the physical properties are affected by shrinking the dimension of ZnO. For example, the conductivity of an NW is different from that of the bulk material. In light of the surface scattering, the resistivity should be large in an NW under the assumption that the band structure does not change. However, experimental studies have shown the opposite indications on this point. There are reports showing the superior mobility observed in ZnO NW devices exceeding state-of-the-art planar devices [12].

In this review, we discuss the surface-related transport, photoluminescence (PL), and photoconductivity properties of ZnO nanostructures. Furthermore, we examine recent studies on the applications of nanostructured ZnO, taking the advantage of the surface effect on gas/chemical sensing, employing the change of conductivity via electron trapping and detrapping process at the surfaces of nanostructures. We also discuss the emerging photovoltaic (PV) application of ZnO nanostructures. The ultrahigh S/V ratios of nanostructured devices suggest that the studies on the synthesis and PV properties of various nanostructured ZnO for dye-sensitized solar cells (DSSCs) offer great potential for high efficiency and low-cost solar cell solutions. At the end of this review, we will address most of the barriers that must be overcome before ZnO nanostructures can reach their ultimate potential as a new class of industrial materials.

TRANSPORT PROPERTIES

The fundamental study in the electrical properties of ZnO nanostructures is demanded for developing the nanoelectronics. The high S/V ratio of ZnO nanostructures makes them suitable for biosensors and chemical sensors with significantly improved sensitivity. Understanding the surface effects, such as geometric properties, surface states, surface roughness, and surface passivation, on the transport behavior of ZnO nanostructures is crucial for reliable device fabrication. Among the various ZnO nanostructures, the transport of individual ZnO NWs/NRs has been extensively investigated [28–34]. Due to the confined geometry of the low-dimension nanostructures, it is not possible to determine the electrical properties by conventional thin-film techniques such as Hall measurements. Alternatively, the measurements of a single ZnO NW-based three-terminal FET are often used to estimate device characteristics, such as the carrier concentration, mobility, effective barrier height, and ideality factor from I-Vmeasurements under different gate voltages [12,13,34-36]. In the typical FET test structures, a pair of leads patterned on the two ends of the NW serves as the source and drain electrodes using conventional photolithography or e-beam lithography. Additionally, a weak capacitively coupled terminal as the gate electrode is employed to control the NW conduction, and thus gates the FET device performances such as operation speed, power efficiency, and ON/OFF ratio by applying a transverse electric field [35,37,38]. There are several types of gate configurations of NW FETs, i.e., back, top, side, and surrounding gates. The back-gate configuration is mostly used due to its simplicity of fabrication. The schematic of a back-gate NW FET with the measurement circuit is shown in Fig. 1. The electron mobility (μ) and the carrier concentration (n) are related to the transconductance ($g_{\rm m} = dI_{\rm ds}/dV_{\rm o}$) and can be calculated as follows:

$$\mu = \frac{dI_{\rm ds}}{dV_{\rm g}} \frac{L^2}{V_{\rm ds} C_{\rm g}} \tag{1}$$

and

$$n = \frac{C_{\rm g} \left| V_{\rm g} - V_{\rm gt} \right|}{e\pi r^2 L} \tag{2}$$

where

$$C_{\rm g} = \frac{2\pi\varepsilon_{\rm r}\varepsilon_0 L}{\cosh^{-1}\left(\frac{r+h}{r}\right)} \tag{3}$$

where $C_{\rm g}$ is the gate-NW capacitance, h is the thickness of the gate insulating layer, L is the NW channel length, r is the NW radius, $\varepsilon_{\rm r}$ is the dielectric constant of the gate insulating layer, $V_{\rm ds}$ is the source-drain voltage, $V_{\rm g}$ is the gate voltage, and $V_{\rm gt}$ is the gate threshold voltage below which current is suppressed to an OFF state [13,35].

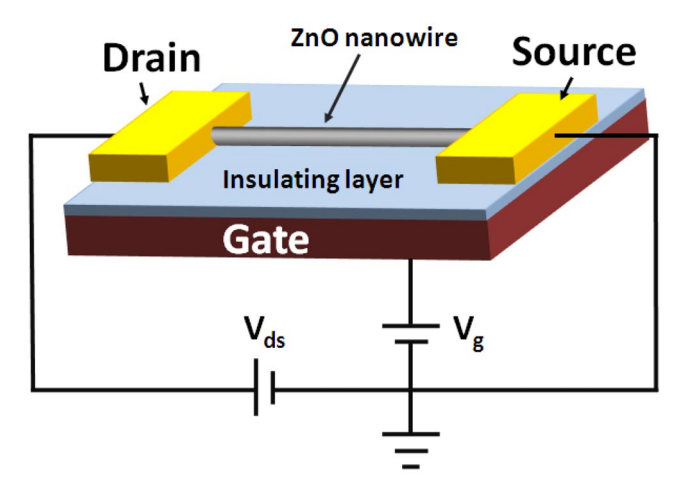


Fig. 1 Schematic of an NW-based FET with the measurement circuit.

Due to the native defects such as oxygen vacancies and zinc interstitials, intrinsic ZnO shows n-type semiconductor behavior. It is well known that the native defects at the metal oxide surfaces serve as the binding sites for chemisorption processes, such as the formations of charged oxygen molecule complexes $[O_2(g) + e^- \rightarrow O_2^-(ad)]$; more details will be discussed in the section on gas/chemical sensors]. They also contribute to the scattering and the trapping of carriers [39], thus lowering the carrier mobility. Furthermore, negative oxygen molecule complexes $[O_2^{-}(ad)]$ adsorbed on the ZnO surfaces form the depletion regions that reduce the conductivity, influencing the operation modes of NW FETs [36]. This unusual behavior comes from the surface band bending [40,41]. It is expected that the surface band bending at the surface of single-crystalline NWs is more pronounced than that in the thin film counterpart [42,43]. As a result, the surface treatment on the ZnO nanostructures is important to tailor the desired electrical characteristics of NW-based devices. ZnO NWs exhibited an electron mobility of 1000 cm²/Vs, which is larger than that of thin film (115–155 cm²/Vs) after coating the NWs with polyimide [34,44]. Using SiO₂/Si₃N₄ as the passivation layer was also found to enhance electron mobility up to $4120 \text{ cm}^2/\text{Vs}$ [12]. In addition to the passivation layer, the post-annealing in ozone [36], O_2 [45], H₂ [46], or N₂ [47] ambient has been applied to enhance the electron mobility. These surface modifications aim for compensating the surface states or reconstructing the surface of NWs and then eliminating the surface scattering and reducing the trapping centers, leading to the enhanced mobility. For example, the electron mobility of an ozone-treated single ZnO NW is up to 1175 cm²/Vs [36]. These results suggest that after the surface modifications, ZnO nanostructure-based devices can achieve a faster operation speed than their thin film counterpart.

The operation modes of transistors (depletion- or enhancement-mode) can be crucially determined by the carrier trapping states at the surfaces [13]. The trapping of electron carriers in the trap states $[O_2(g) + e^- \rightarrow O_2^-(ad)]$ can cause electron depletion in the channel, resulting in a gate threshold voltage shift and a conductance modulation. The rough NWs have more fraction of the surface depletion region in the NW channel than the smooth ones. Depletion- and enhancement-mode FETs were demonstrated by the smooth and rough surfaces of ZnO NW FETs, respectively [13]. Both depletion- and enhancement-mode FETs are demanded for NW-based integrated-circuit electronics with the high logic performance. The inverter circuits, by combination of both depletion- and enhancement-mode ZnO NW devices, exhibit the desired voltage-transfer characteristics with high gains, robust noise margins, and less power dissipation, which makes them superior to logic inverters based on single-mode NW FETs [48]. However, the rough surface of NWs may cause carrier scattering, leading to the limited operation speed. In order to maintain the operation speed, the depletion in the NW channel could be generated by the appropriate coating layer instead of the rough surface of the NWs. ZnO nanostructures will have the opportunity to achieve the electronic devices with less power dissipation and faster operation speed by the surface modifications.

PHOTOLUMINESCENCE PROPERTIES

Room-temperature PL analysis is widely used to investigate the optical properties of ZnO. Optical properties of various ZnO nanostructures are intensively studied since it has been realized that ZnO is the ideal material for light emitters mainly due to its tightly bound excitons and wide bandgap, which lead to highly efficient near-band-edge recombination at UV regions [24,27,49–97]. Different nanostructures show some variations of the position and the intensity of the peak in the PL spectra. Room-temperature near band-edge emission (NBE) in the different ZnO nanostructures has been reported to occur at 373 [50], 378 [51–53], 380 [54–56], 381 [57], 383 [58,59], 384–391 [60], 387.5 [61], 389 [59,62], and 390 nm [63]. Size-dependent time-resolved PL (TRPL) analysis indicates that the defect densities of the various nanostructures with high S/V ratio are varied as compared with the bulk ZnO [27,64,65], leading to the distinct shifts of the NBE for a variety of nanostructures synthesized by different methods [49]. Furthermore, although the sizes of these ZnO nanostructures are larger than the Bohr radius of ZnO [66], the blue-shift of NBE in ZnO nanostructures is observed by decreasing the size of ZnO nanocrystals (NCs) [67], nanodots [68], and NBs [69], which is indicative of surface effects as well. For the sizes of ZnO structures larger than the Bohr radius, it is suggested that the variations in the position of the NBE in various ZnO nanostructures result from different concentrations of native defects. Roomtemperature PL spectra of ZnO typically exhibit the visible emission, which corresponds to the deeplevel emission (DLE). Figure 2 shows the DLE (normalized PL spectra) from different ZnO nanostructures, which results from the various defect states, as shown in Fig. 3. The defect ionization energies range from ~0.05 to 2.8 eV [70,71]. The green emission is the most commonly observed defect emission in ZnO nanostructures [50,52-54,56,58-61,72-76] and often attributed to singly ionized oxygen vacancies [50,54,55,73,76], donor–acceptor transitions [77], recombination at V_0 enters [78,79], zinc vacancies [80,81], and surface defects [82]. Although the defect origin of the green emission has not been conclusively identified, polarization-dependent PL spectra from aligned ZnO NRs have demonstrated that green emission originates from the NR surfaces [83]. It has been shown that coating ZnO nanostructures with the surfactant can suppress the green emission significantly [82]. The thickness of surface recombination layer responsible for visible emission in ZnO NWs is estimated to be ~30 nm [27]. Therefore, it is confirmed that the green emission comes from ZnO surfaces.

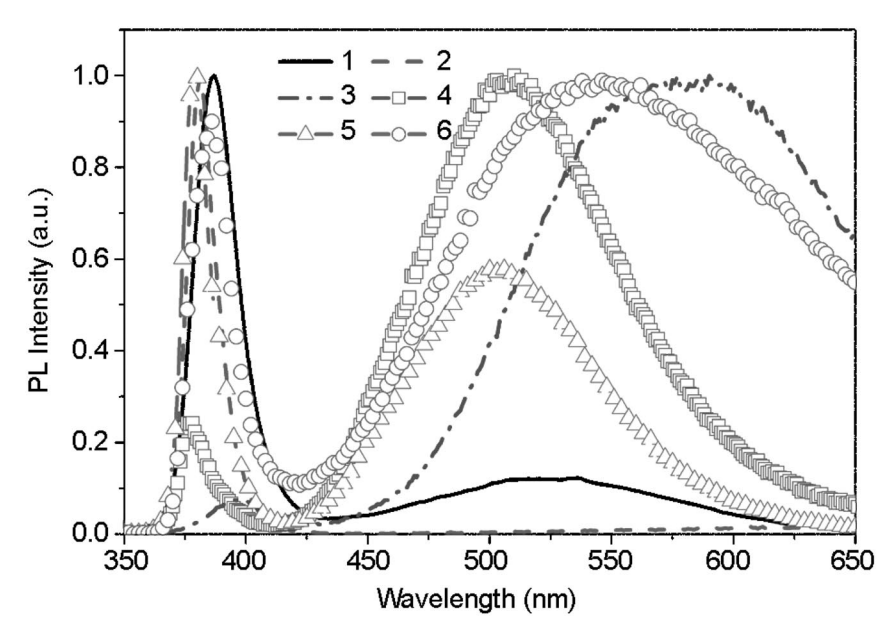


Fig. 2 Room-temperature PL spectra of various nanostructures in the UV range: (1) tetrapods, (2) needles, (3) NRs, (4) shells, (5) highly faceted rods, (6) ribbons/combs. Reprinted with permission from ref. [49]. Copyright © 2006 John Wiley.

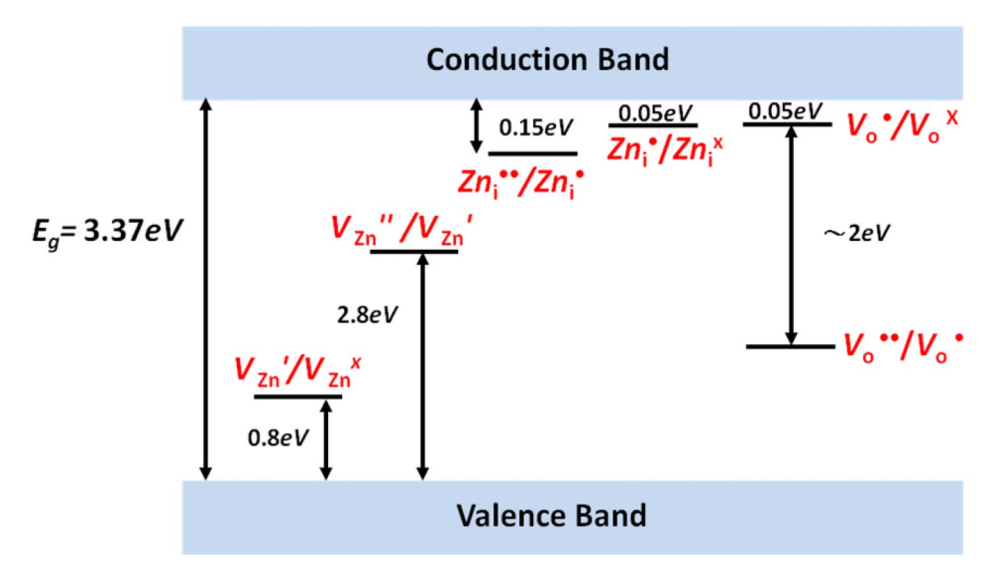


Fig. 3 Energy levels of native defects in ZnO. The donor defects are $Zn_i^{\bullet\bullet}$, Zn_i^{\bullet} , Zn_i^{\bullet} , Zn_i^{\bullet} , $V_0^{\bullet\bullet}$, V_0^{\bullet} , and the acceptor defects are V_{Zn}'' , V_{Zn}' . The Kroger Vink notation uses: i = interstitial site, Zn = zinc, O = oxygen, and V = vacancy. The terms indicate the atomic sites that the species occupy, and superscripted terms indicate the electronic charges of the species relative to the site that it occupies, where a dot indicates positive charge, a prime indicates negative charge, and a cross indicates zero charge, with the charges in proportion to the number of symbols. Reprinted with permission from ref. [142]. Copyright © 1974 American Elsevier.

In addition, the intensity of the blue–green defect emission depends on the NW diameter [56,84], but both increased and decreased intensities of defect emissions have been observed with the diameter [56,84]. However, the blue–green defect emissions can be attributed to singly ionized oxygen vacancies since the intensity of the blue–green emission is increased with S/V ratio [56,84]. The yellow emission attributed to oxygen interstitials is commonly observed in ZnO nanostructures as well [51,59,80,85]. The defect responsible for the yellow emission is not located at the surface [59,85] and can be eliminated by annealing in hydrogen/argon ambient [51]. However, the aforementioned has demonstrated that ZnO nanostructures have potential for a tunable-wavelength LED material by the shift of the NBE and DLE due to different S/V ratios.

Various complex nanostructures have been synthesized to tailor the optical properties since the engineering of the ZnO NWs/NRs through surface modification can maximize the benefits provided by nanostructures [86–90]. For example, the enhancement of PL has been observed in ZnO/Er $_2$ O $_3$ and ZnO/ZnMgO core-shell nanostructures [87,88]. An aqueous chemical method was also proposed to fabricate the well-aligned ZnO/Al $_2$ O $_3$ core-shell NRs. The Al $_2$ O $_3$ shell layer resulting in the flat-band effect near the ZnO surfaces leads to a stronger overlap of the wavefunctions of electrons and holes in the ZnO core, further enhancing the NBE [24]. The PL intensity of ZnO/ZnS nanotetrapods and the lifetime of the UV exciton radiative transition have been increased by more than 20 times due to the passivation effect of the core-shell structures [91]. The shell layer not only can make a strong overlap of the wavefunctions but also can compensate the surface states of the NWs, leading to enhancement of the NBE emission. In addition, the appropriate shell layer can avoid oxygen adsorption/desorption (more details will be discussed in the section on gas/chemical sensors) to make the luminescent properties of ZnO stable.

In addition to the room-temperature PL analysis, the low-temperature PL measurements are often applied to investigate exciton emissions in ZnO nanostructures with high efficient recombination. Due to the high absorption coefficient for photons of $hv > E_g$, where E_g is the bandgap energy, most of the excitons and carriers are generated near the semiconductor surfaces. In the case of ZnO nanostructures, a large fraction of free excitons can be bound to the surface defects. The excitons localized in surface states near the surfaces within the thickness of ~20 nm are defined as surface excitons (SXs) [92,93]. Due to the surface band bending, the photon energy of SXs is higher than that of other bound excitons but lower than that of free excitons [94,95]. As the power intensity of photo-excitation is increased, the saturation behavior in the PL intensity of SXs can be readily observed, which is different from other bound excitions [94]. When the size of ZnO nanostructures is decreased, the role of SXs becomes important for the optical and electronic properties of ZnO [94,96,97]. The enhanced SX emission at helium temperature has been demonstrated in ZnO/amorphous Al₂O₃ core-shell NWs because a reduced band bending generated the high density of SX near the surfaces [89]. Because the photon emissions from ZnO closely correlate with ZnO surfaces and SX is one of the dominant surface-related emissions, the core-shell nanostructure can provide a platform to investigate the surface-related emission in detail by applying different materials and thicknesses of shell layers. This would benefit the development of ZnO nanostructures for optoelectronic nanodevices.

PHOTOCONDUCTIVITY PROPERTIES

For ZnO thin-film-based UV detectors, a slow response time ranging from a few minutes to several hours and a low optical gain are commonly observed. However, ZnO nanostructures show significantly improved performances of photodetectors. It has been reported that the internal photoconductive gain of intrinsic ZnO NW-based UV photodetectors could be as high as $\sim 10^8$ due to the presence of the oxygen-related hole-trapping states (i.e., oxygen vacancies) at NW surfaces [17,19,98]. Because the photogenerated holes are trapped at the hole trapping states $[O_2^-(ad) + h^+ \rightarrow O_2(g)]$, the life times of the photogenerated electrons are increased. In addition, photoconductivity was also observed at energies corresponding to the deep-level states confirmed by PL spectra. Photocurrent as a function of the light

polarization angle for both UV and visible light has been demonstrated, as shown in Fig. 4 [19]. Polarized photodetection of both UV (365 nm) and visible light shows that the photoconductivity of ZnO NW is maximized when the incident light is polarized parallel to the NW axis. This behavior specifies ZnO NWs, promising application in high-contrast polarizer. Photoresponses of the ZnO NWs under the illumination of above-bandgap light (325 nm) and defected-related light (453 nm) are significantly different in the maximum photocurrent while they both exhibit slow photoresponses, as shown in Fig. 5. According to the photoconductivity studies of ZnO NWs, the presence of O₂ has an important effect on the photoresponse [32,99]; i.e., O_2 adsorption on the NW surface $[O_2(g) + e^- \rightarrow O_2^-(ad)]$ could significantly hasten the photocurrent relaxation rate. As shown in Fig. 6, the photocurrent relaxation time is hours in vacuum but around 8 s in air ambient. This is the oxygen-related hole-trapping state effect. Upon illumination, the photogenerated holes discharge surface chemisorbed O2 through electron-hole recombination at the surfaces $[O_2^-(ad) + h^+ \rightarrow O_2(g)]$, which increases the time it takes electrons and holes to recombine and thus trigger an increase in the photoconductivity. By blocking the illumination, O₂ molecules re-adsorb onto the NW surface and reduce the photoconductivity. Recently, researchers' attention has been focused on improving the responses and reset times. The UV response of a ZnO NB-based sensor has been enhanced by five orders of magnitude after functionalizing its surface with a polymer layer for UV absorption [100,101]. This giant enhancement is suggested to the energy levels introduced by the polymer lying in the corresponding bandgap and in the conduction band of ZnO, which serve as a "hopping" state and increase the excitation probability of an electron to the conduction band. The reset time of ZnO NW-based photodetector has been reduced drastically by surface functionalizing or utilizing a Schottky contact [102,103]. The slow recovery time of the NW-based photodetector is attributed to O_2 molecule re-adsorbtion onto the NW $[O_2(g) + e^- \rightarrow O_2^-(ad)]$. Therefore, the reset time benefits by speeding up the process of O₂ molecules re-adsorbing.

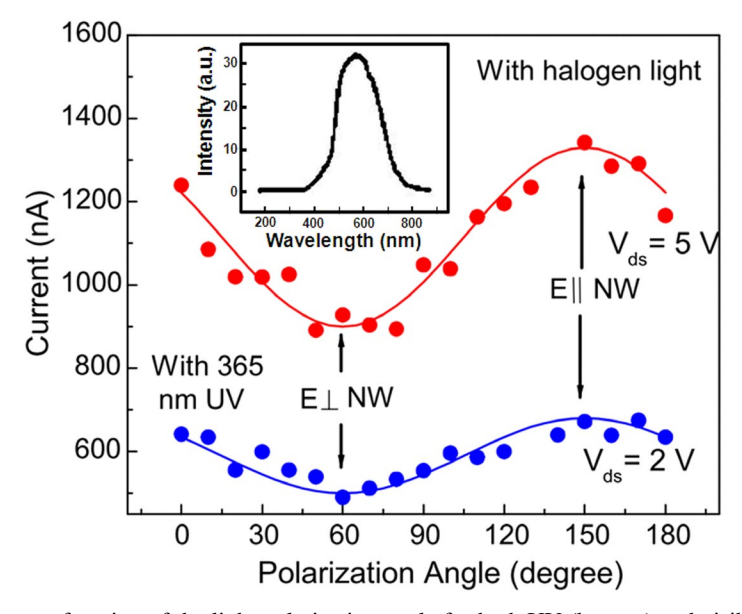


Fig. 4 Photocurrent as a function of the light polarization angle for both UV (bottom) and visible light (top). The inset shows a spectrum of halogen light source. Reprinted with permission from ref. [19]. Copyright © 2004 American Institute of Physics.

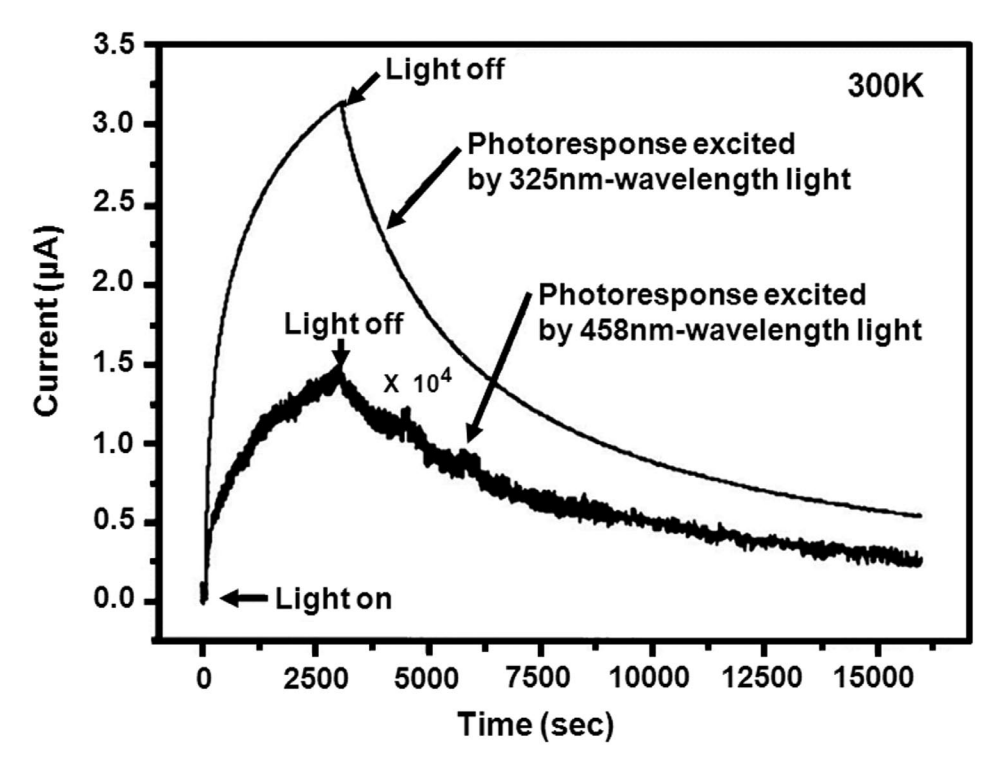


Fig. 5 Photoresponse of the ZnO NWs under the continuous illumination of 325- and 458-nm wavelength light and after turning off the light in vacuum at 300 K at a bias voltage of 0.5 V. Reprinted with permission from ref. [99]. Copyright © 2004 American Institute of Physics.

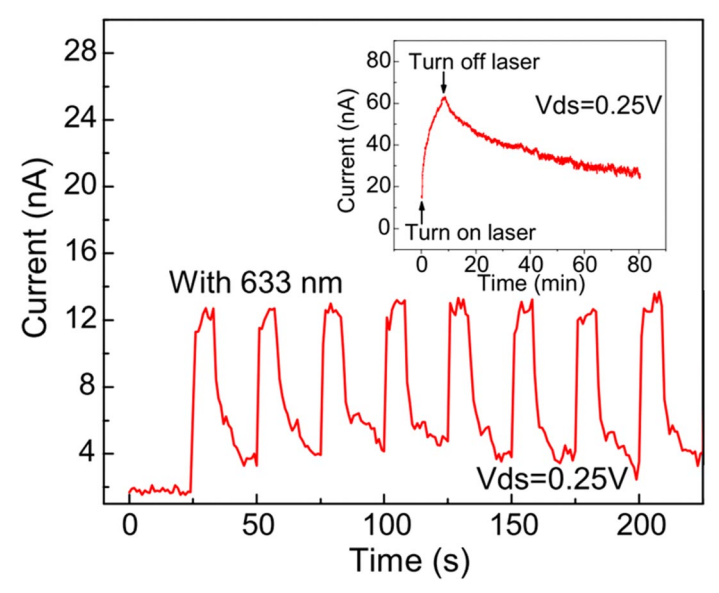


Fig. 6 NW photoresponse to 633-nm laser in air compared to that in vacuum (inset). Reprinted with permission from ref. [19]. Copyright © 2004 American Institute of Physics.

GAS/CHEMICAL SENSORS

ZnO NWs are also useful in detecting versatile gases due to their high S/V ratios. The fundamental mechanism relies on a change of conductivity via the electron trapping and detrapping process on NW surfaces. Ambient conditions, intrinsic oxygen vacancies, and sensing temperatures which significantly influence surfaces play important roles in the response time of gas-sensing detectors [104–108]. As gas molecules are adsorbed on NW surfaces, charge transfer occurs and modifies the carrier concentration, resulting in a change of conductivity. For NO₂ or O₂, they tend to capture free electrons in NWs and dissociate into NO₂⁻ or O₂⁻, forming a low-conductivity depletion layer near the surfaces. Therefore, the conductivity of ZnO NWs is decreased in the presence of NO₂ and O₂ [109–113]. On the other hand, reductive gases, such as ethanol, H₂, CO, and H₂S, react with the charged oxygen molecules on NW surfaces, and thus free electron concentration is increased due to oxygen desorption $[O_2^-(ad) \rightarrow O_2(g) + e^-]$, leading to an increase of conductivity [104–106,114,115].

ZnO NWs with various sizes for gas sensing have also been reported. As the NW diameter shrinks, the sensitivity to oxygen sensing is increased due to the large S/V ratio and the high density of oxygen vacancies in NWs [108,112]. It is believed that the majority of oxygen vacancies exist at the surface of NW and act as adsorption sites for oxygen molecules [84], which adsorb on the ZnO NW surface by capturing free electrons from the n-type ZnO, thereby creating a depletion layer with low conductivity near the surface $[O_2(g) + e^- \rightarrow O_2^-(ad)]$. The reason for high density of oxygen vacancies in small NWs is that the compressive stress within ZnO NWs increases with the decreasing diameters of NWs and thus increases the density of oxygen vacancies in the surface layers of the NWs [116]. Consequently, a large quantity of oxygen vacancies and large effective surface areas at the surfaces of NWs with small diameter lead to the serious depletion layers near the surfaces. This enhanced sensitivity for ZnO NWs with small diameters can be explained by a surface depletion layer-dominated mechanism [117]. The formation of the depletion regions near NW surfaces reduces the carrier concentration and thus has a great influence on NW conductivity especially when the NW diameter is comparable to the Debye screening length [117,118]. In the presence of reductive gases, electrons trapped on the surface are released by oxygen desorption $[O_2^-(ad) \rightarrow O_2(g) + e^-]$, resulting in a great change of the conductivity and the width of surface depletion region. This change is more prominent for NWs with small diameters, leading to the significant increase of sensitivity of gas sensing [117,119]. A similar concept of enhancing the sensitivity by reducing carrier concentration has been achieved with the oxygen plasma treatment for NH₃ sensing [120].

ZnO NW FETs for gas sensing have also been fabricated to enhance the sensitivity via adjusting the gate voltage to affect gas adsorption/desorption behavior at NW surfaces. With the aid of a negative bias to deplete the electrons in NWs, the binding of oxygen adsorption is weakened, resulting in a sensitivity improvement for NO₂ and NH₃ sensing. Furthermore, a strong negative bias can refresh the gas sensors, and the selectivity of gas sensing can be carried out by refreshing the threshold voltage [118]. The aforementioned results open the possibility of a single NW-based gas/chemical sensor with wide-detection range and high sensitivity by tunable gate voltage.

Response and reset times are among the critical figures of merit for gas/chemical sensors. For the two figures of merit, there are several surface-related improvement methods, such as the formation of Schottky contact and the surface modification on ZnO nanostructure-based devices [121]. Regarding the Schottky contacted NW gas sensor, Fig. 7 shows the proposed mechanism. In the presence of oxygen molecules, the Schottky barrier height is further increased due to oxygen adsorption, resulting in a dramatic reduction of conductivity. For CO sensing using this method, CO molecules react with the adsorbed oxygen molecules and release the trapped electrons, leading to the fact that the Schottky barrier height is decreased with a drastic current recovery, and the response time and the reset time can also be reduced [121].

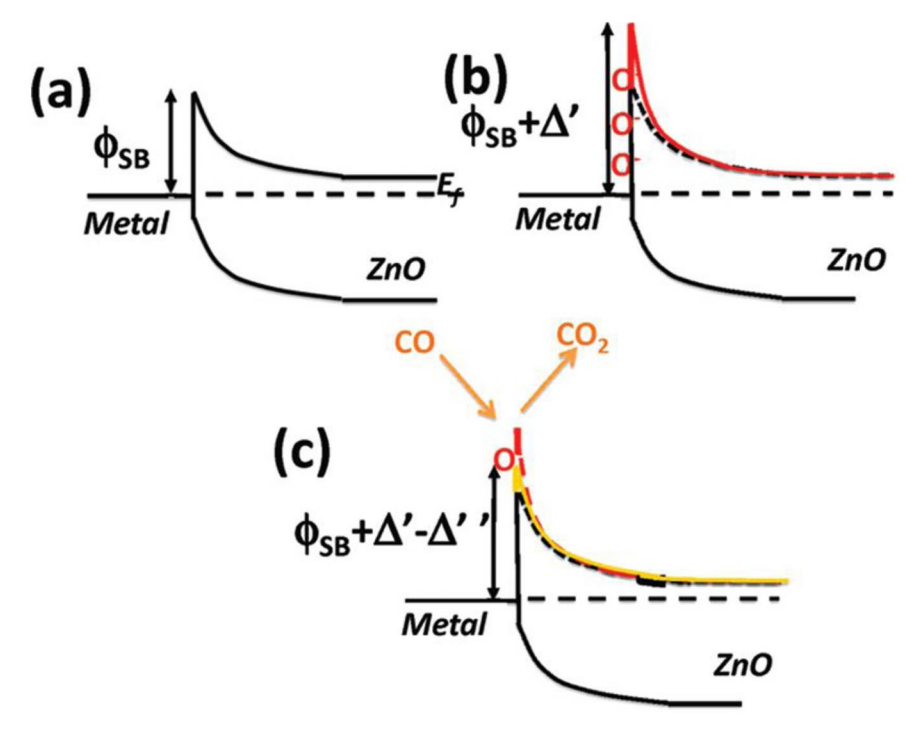


Fig. 7 Sensing mechanism of a variable Schottky barrier height, corresponding to different conditions: in (a) N_2 , (b) O_2 , and (c) CO ambient. Reprinted with permission from ref. [121]. Copyright © 2009 American Chemical Society.

Several surface modification techniques have been used to improve the gas sensing performances of ZnO nanostructures because of their strong surface-related sensing behavior. Au NP-decorated ZnO NWs for CO sensing have been studied. Au NPs on NW surfaces act as the catalyst in the process of reducing the activation energy for oxygen dissociation and spilling the charged oxygen molecules over the NW surfaces due to their availability of free electrons and highly conductive nature, resulting in the improved gas-sensing behavior. This mechanism is also known as spill-over effect [104,122,123]. Due to the large difference between the work function of Au and the electron affinity of ZnO, Au NPs also enhance the surface depletion effect by modulating the surface depletion region and account for the rapid and ultrahigh sensing for ethanol [119,123]. Pt NP-decorated ZnO NWs are also found to be effective in enhancing the response to H₂S and ethanol [16,124]. As shown in Fig. 8, the response increases with H₂S concentration, and can be further enhanced by Pd NP decoration. The sensitivity of acetone and toluene sensing using InSb- and TiO₂-doped ZnO NWs have been improved by the surface modification, which reduces the activation energy of oxygen desorption and thus efficiently desorbs oxygen molecules at the surfaces of ZnO NWs [125,126]. A reduction of activation energy also contributes to the reduction of response and reset times [118]. The enhanced sensitivity in a bilayered polymer/ZnO gas sensor based on the ZnO NBs with a plasma-polymerized acrylonitrile (PP-AN) surface coating has been observed as well [107]. PP-AN can increase the concentration of the adsorption sites for target gases, resulting in a high sensing response. Moreover, it has been reported that desorbing charged oxygen molecules adsorbed at NB surfaces using UV illumination can create more adsorption sites for subsequent oxygen molecules sensing, leading to the improvement of sensitivity [107].

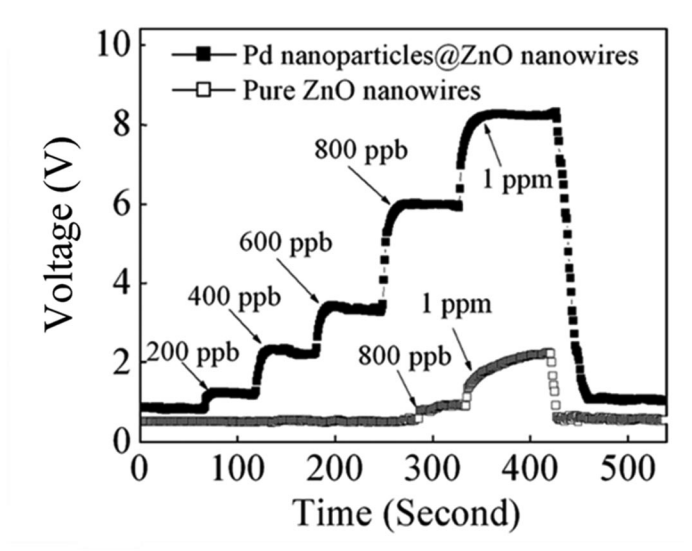


Fig. 8 Dynamic responses of sensors with different samples to H_2S . Reprinted with permission from ref. [124]. Copyright © 2009 Royal Society of Chemistry.

DYE-SENSITIZED SOLAR CELLS

DSSCs were reported by Grätzel et al. in 1991 [127]. As they are one of the most promising low-cost solar cells, a lot of work has been done to try to improve their performance. DSSCs are based on photo-excitation of dye molecules at the surfaces of the metal oxide electrodes, such as ZnO. Electrons are injected from the dye molecules into the metal oxide electrodes, and the dye is reduced by electron donation from the electrolyte. Therefore, the metal oxide electrodes are investigated intensively for achieving a fast electron transport and improving the efficiency of DSSCs [21,128,129]. TiO₂ is the most widely used electrode in DSSCs. However, ZnO is thought to be a potential substitute for TiO₂ due to its high mobility [44].

Since light absorption plays a dominant role in the operation of solar cells, increasing the cross-section area of optical absorption is usually the first step in the work of improving solar cell efficiency. The nanostructures with high S/V ratio can be beneficial in this regard. A dye monolayer on a flat interface for ZnO thin films exhibits only negligible light absorption since the cross-section of optical absorption for molecular dyes is typically 2–3 orders of magnitude smaller than their physical cross-sections. The use of a nanostrucured ZnO can significantly enhance the interfacial surface area over the geometric surface area, by up to 1000-fold for a 10- μ m-thick film, leading to high absorbance from the many successive monolayers of adsorbed dyes in the optical paths [130]. Figure 9 shows the schematic of ZnO nanostructure-based DSSCs. To compare with TiO₂, ZnO can be easily fabricated in various morphologies with a large surface area, which is the essential factor in maximizing dye adsorption. In general, the I_{sc} is proportional to the amount of the absorbed dyes, which are related to the area of the electrodes of DSSCs. The roughness factor (RF), defined as the ratio of total surface area of electrodes to the shadow substrate area of a cell, is widely used to quantitatively estimate the amount of the absorbed dyes [21]. Various ZnO nanostructures used in DSSCs and their performance are listed in Table 1.

Table 1 Performance of DSSCs utilizing different ZnO nanostructures.

Nanostructure	η (%)	$V_{\text{oc}} (\text{mV})$	$I_{\rm sc}~({\rm mA/cm^2})$	FF	Refs.
Nanocrystalline film	0.40	550	1.22	0.66	[143]
	2.80	550	9.10	0.57	[144]
NR	1.32	570	7.00	0.33	[145]
	4.70	710	10.70	0.62	[144]
Nanofiber	3.02	570	9.14	0.58	[146]
NW	1.50	710	5.85	0.38	[21]
	0.84	500	3.40	0.49	[22]
NW with branched structure	0.46	620	1.84	0.40	[147]
NW with pillar structure	0.34	690	1.26	0.39	[147]
Nanosphere	1.59	668	5.43	0.44	[136]
	2.60	557	12.30	0.48	[148]
Nanotetrapod	1.02	580	3.76	0.47	[149]
	3.27	614	9.71	0.55	[150]
Nanoflower	1.60	580	8.75	0.32	[137]
	0.30	535	1.10	0.54	[148]
Nanoflower with Au NPs	2.50	500	15.00	0.33	[137]
NP	0.87	670	2.25	0.58	[145]
	6.58	621	18.11	0.59	[135]
	0.75	573	1.20	0.51	[151]
Nanosheet	1.55	593	2.06	0.55	[151]
Mesoporous aerogel thin films	2.40	600	8.32	0.48	[152]
NP aggregate	5.40	595	9.70	0.45	[153]
Plate aggregate	1.90	554	8.40	0.41	[148]
Network structure	1.34	600	3.58	0.62	[154]
Hierarchical structure	6.51	670	10.90	0.48	[155]
Nanosphere/film composite	2.25	718	6.13	0.51	[136]
NW/NP composite	2.20	610	6.30	0.58	[22]
ZnO/TiO ₂ core/shell NW	2.27	800	4.78	0.60	[139]
-	2.00	705	5.30	0.54	[140]
	2.00	704	5.30	0.53	[141]

 η is solar energy conversion efficiency, $V_{\rm oc}$ is open-circuit voltage, $I_{\rm sc}$ is short-current density, FF is fill-factor, NPs is nanoparticles, and NWs is nanowires.

For DSSCs, the electron transport of ZnO is also related to its morphologies [21,131–134]. For example, the electron transport in the ZnO NW DSSCs is about two orders of magnitude faster than that in the ZnO NP DSSCs [131]. However, the short-circuit photocurrent density ($I_{\rm sc}$) and the energy conversion efficiency (η) of ZnO NP DSSCs (with 22.8 μ m in thickness) are superior to those of the ZnO NW DSSCs (with 18~24 μ m in length) [21,135]. This can be explained as follows: the RF of 882.35 for ZnO NP DSSCs is much larger than that for ZnO NW DSSCs (RF = 200) [21,135]. If the RF is sufficiently large, even a monolayer of dye molecules could absorb most of the incident photons [127]. Therefore, it is a trade-off problem of improving the efficiency by varying the morphology of ZnO electrodes.

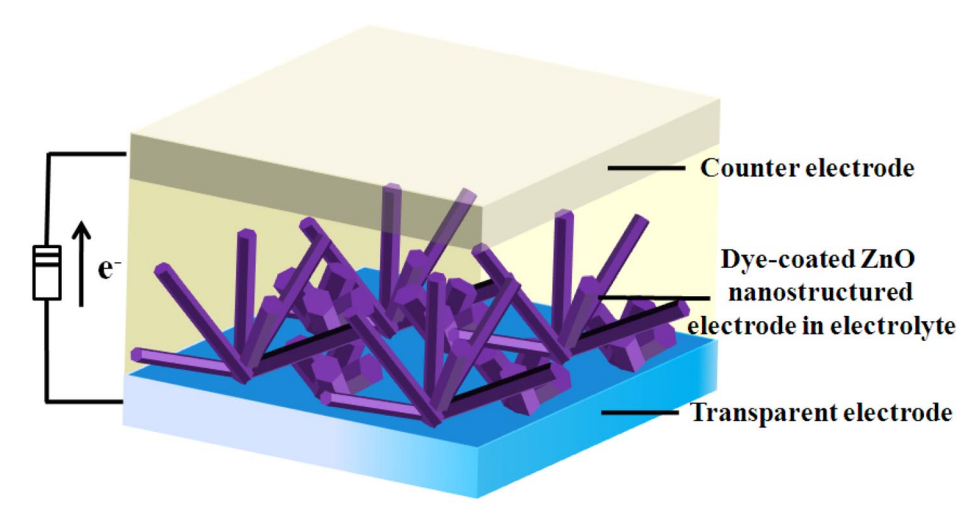


Fig. 9 Schematic of ZnO nanostructure-based DSSCs.

The transport in DSSCs is influenced by the surfaces of nanostructured electrodes as well. For example, some electrons might be captured by the surface states located on the ZnO electrode surface, decreasing the η of the cell. Surface passivation, which can reduce the surface defects of the ZnO, is another method to enhance the η . After annealing the ZnO electrodes in oxygen ambient, the η increases from 1.03 to 1.59 % [136]. Au NPs have been found to enhance the η of ZnO nanoflower-based DSSCs; i.e., the ZnO nanoflowers decorated with Au NPs showed 2.5 % of η , higher than 1.6 % for the ZnO nanoflowers [137]. This is because surface defects are eliminated during the Au NPs' formation process, possibly by the electron abstraction from the defects through the reduction of Au ions.

Moreover, ZnO surface is unstable in acidic dye of DSSCs, such as N3 and N719. ZnO surface forms Zn²⁺/dye complexes in the dye environments, leading to a low electron injection efficiency of the dye molecules [138]. The core-shell structure, one of the surface passivation methods, provides a good way to protect the ZnO against the harm of the acidic dye. The Al₂O₃ shells acting as a protecting and electron-blocking layer improved the open-circuit voltage ($V_{\rm oc}$) but greatly decreased the short-circuit current of the ZnO/Al₂O₃ core-shell NW DSSCs [139]. However, TiO₂ shells increased the $V_{\rm oc}$ and fill factor, resulting in the improvement of η up to 2.25 % for the ZnO/TiO₂ core/shell NW DSSCs [139]. This is due to the fact that the shells suppress the recombination by forming an energy barrier and passivating surface recombination centers [140,141]. Therefore, surface treatments, such as coating shell layer or decoration with metal particles, can improve the efficiency and the endurance of DSSCs. However, the influence on $V_{\rm o}$ and $I_{\rm sc}$ should also be considered when improving the efficiency.

CONCLUSION AND OUTLOOK

We have reviewed some of the critical, initial research designed to determine unique transport, PL, and photoconductivity properties offered by ZnO nanostructures with ultrahigh S/V ratio. Preliminary works from many research groups demonstrate that there are many applications of nanostructured ZnO devices in electronics and optoelectronics. After showing some of the empirical information accumulating in the current literature on the surface effects on nanostructured ZnO, we believe that there are a few surface-related issues that remain to be addressed before nanostructured ZnO devices can reach their ultimate potential as a new class of industrial applications.

First of all, nanostructure is not simply a miniaturization in sizes. To conclusively identify the surface effects, powerful tools must be established to measure atomic structure, understand local electronic structure, and detect local chemistry at the ZnO surfaces precisely.

The second challenge is that the chemical/thermal stability of nanostructured ZnO still needs to be controlled well and studied systematically. Although various methods for controlling surface effects, such as heat treatments and surface functionalization, have been applied, comprehensive study on the relationship between processes conditions and surface effect is still needed. For instance, as discussed before, when deposited on the surface of nanostructured ZnO, the passivation layers could compensate the surface states or reconstruct the surfaces of nanostructured ZnO, leading to chemical stability in some way. However, the ultimate utilization of nanostructured ZnO devices strongly depends on the ability to precisely control surface properties with durability. Judged against these metrics, the demand for the research work on the effect of surface treatment will certainly be increased before finding widespread use in practical applications. Moreover, it has been known that when the size of nanomaterials is decreased greatly, the melting point will be reduced significantly due to ultralarge surface areas as compared to the bulk materials. This weakened thermal stability may severely limit the use of nanostructured ZnO.

The third challenge is the feasible scheme for controlled growth of nanostructured ZnO. Nanostructured ZnO is being used increasingly as 1D building blocks in electronics and optoelectronics of the future, taking advantage of the surface-dependent physical properties of ZnO. Considerable effort must be devoted to developing nanostructured ZnO building blocks of controlled geometry, such as diameters, lengths, surface roughnesses, and predetermined configuration since surface effects are pronounced in nanostructured ZnO. We are convinced that the ability to fabricate ordered nanostructures of ZnO with desirable geometry would provide a useful platform for the fundamental understanding of surface effects and represent one of the critical steps toward the feasibility of practical applications of nanostructured ZnO.

The fourth challenge is the achievement of reliable *p*-type ZnO. Without question, the most significant impediment to the widespread exploitation of ZnO in electronic and photonic applications is the difficulty in achieving *p*-type ZnO due to the presence of intrinsic defects in ZnO. Even if acceptors are deliberately added in ZnO, donors are easily formed as compensation centers and tend to be dominant; i.e., *p*-type ZnO changes back to *n*-type over time due to its instability, although some studies have demonstrated an incontrovertible proof that *p*-type ZnO indeed exists. The wide variety of growth techniques for *p*-type nanostructured ZnO is needed urgently for enhancing the commercial appeal of nanostructured ZnO. The condition of nanostructured ZnO growth can lead to various types of acceptors and donors at the surfaces, which significantly influence electrical and optical properties of ZnO; thus, the research on the surface effect on physical properties of nanostructured *p*-type ZnO is crucial as well.

Although the properties of various nanostructures are similar to those reported for thin films, the pronounced surface effect significantly enhances electrical and optical properties; i.e., the observed size effects in nanostructures are the result of different S/V ratios rather than quantum confinement. Nanostructured ZnO and its applications derived from the surface effects are still in an early stage of technical development. The ability to manipulate the phenomena due to the surface effect is demanded. We believe that the promising applications together with a fundamental interest in nanomaterials will continuously provide compelling motivation for research into techniques for fabricating nanostructured ZnO devices with better controlled surface effects. We expect that nanostructured ZnO employing the surface effect could open up the promising potential for future electronic and optoelectronic devices.

ACKNOWLEDGMENTS

The research was supported by the National Science Council Grant No. NSC 96-2112-M-002-038-MY3, NSC 96-2622-M-002-002-CC3, and Aim for Top University Project from the Ministry of Education.

REFERENCES

- 1. L. E. Greene, M. Law, D. H. Tan, M. Montano, J. Goldberger, G. Somorjai, P. Yang. *Nano Lett.* 5, 1231 (2005).
- 2. E. A. Meulenkamp. J. Phys. Chem. B 102, 5566 (1998).
- 3. J. Shi, S. Grutzik, X. Wang. ACS Nano 3, 1594 (2009).
- 4. J. Y. Lao, J. G. Wen, Z. F. Ren. Nano Lett. 2, 1287 (2002).
- 5. X. Y. Kong, Z. L. Wang. Nano Lett. 3, 1625 (2003).
- 6. X. Y. Kong, Z. L. Wang. Appl. Phys. Lett. 84, 975 (2004).
- 7. X. Y. Kong, Y. Ding, R. S. Yang, Z. L. Wang. Science 303, 1348 (2004).
- 8. J. H. He, C. H. Ho, C. W. Wang, Y. Ding, L. J. Chen, Z. L. Wang. Cryst. Growth Des. 9, 17 (2009).
- 9. J. H. He, C. H. Ho. Appl. Phys. Lett. 91, 233105 (2007).
- 10. J. H. He, S. T. Ho, T. B. Wu, L. J. Chen, Z. L. Wang. Chem. Phys. Lett. 435, 119 (2007).
- 11. S. N. Cha, J. E. Jang, Y. Choi, G. A. J. Amaratunga, G. W. Ho, M. E. Welland, D. G. Hasko, D.-J. Kang, J. M. Kim. *Appl. Phys. Lett.* **89**, 263102 (2006).
- 12. P.-C. Chang, Z. Fan, C.-J. Chien, D. Ronning, C. Stichtenoth, J. G. Lu. *Appl. Phys. Lett.* **89**, 133113 (2006).
- 13. W.-K. Hong, G. Jo, S.-S. Kwon, S. Song, T. Lee. *IEEE Trans. Electron Devices* **55**, 3020 (2008).
- 14. J. Bao, M. A. Zimmler, F. Capasso. Nano Lett. 6, 1719 (2006).
- 15. Z. Fan, J. G. Lu. IEEE Trans. Nanotechnol. 5, 393 (2006).
- 16. T.-J. Hsueh, S.-J. Chang, C.-L. Hsu, Y.-R. Lin, I.-C. Chen. Appl. Phys. Lett. 91, 053111 (2007).
- 17. C. Soci, A. Zhang, B. Xiang, S. A. Dayeh, D. P. R. Aplin, J. Park, X. Y. Bao, Y. H. Lo, D. Wang. *Nano Lett.* **7**, 1003 (2007).
- 18. H. Kind, H. Yan, B. Messer, M. Law, P. Yang. Adv. Mater. 14, 158 (2002).
- 19. Z. Fan, P. Chang, E. C. Walter, C. Lin, H. P. Lee, R. M. Penner, J. G. Lu. *Appl. Phys. Lett.* **85**, 6128 (2004).
- 20. S. W. Chan, R. J. Barille, M. Nunzi, K. H. Tam, Y. H. Leung, W. K. Chan, A. B. Djurišić. *Appl. Phys. B* **84**, 351 (2006).
- 21. M. Law, L. E. Greene, J. C. Johnson, R. Saykally, P. Yang. Nat. Mater. 4, 455 (2005).
- 22. C. H. Ku, J. J. Wu. Appl. Phys. Lett. 91, 093117 (2007).
- 23. J. H. He, S. Singamaneni, C. H. Ho, Y. H. Lin, M. E. McConney, V. V. Tsukruk. *Nanotechnology* **20**, 065502 (2009).
- 24. C. Y. Chen, C. A. Lin, J. H. He. Nanotechnology 20, 185605 (2009).
- 25. J. Suehiro, N. Nakagawa, S.-I. Hidaka, M. Ueda, K. Imasaka, M. Higashihata, T. Okada, M. Hara. *Nanotechnology* **17**, 2567 (2006).
- 26. Q. H. Li, T. Gao, Y. G. Wang, T. H. Wang. Appl. Phys. Lett. 86, 123117 (2005).
- 27. I. Shalish, H. Temkin, V. Narayanamurti. Phys. Rev. B 69, 245401 (2004).
- 28. P. Chang, Z. Fan, W. Tseng, D. Wang, W. Chio, J. Hong, J. G. Lu. Chem. Mater. 16, 5133 (2004).
- 29. H. Chik, J. Liang, S. G. Cloutier, N. Kouklin, J. M. Xu. Appl. Phys. Lett. 84, 3376 (2004).
- 30. C. H. Liu, W. C. Yiu, F. C. K. Au, J. X. Ding, C. S. Lee, S. T. Lee. *Appl. Phys. Lett.* **83**, 3168 (2003).
- 31. Q. H. Li, Q. Wan, Y. X. Liang, T. H. Wang. Appl. Phys. Lett. 84, 4556 (2004).
- 32. Y. W. Heo, L. C. Tien, D. P. Norton, B. S. Kang, F. Ren, B. P. Gila, S. J. Pearton. *Appl. Phys. Lett.* **85**, 2002 (2004).
- 33. M. S. Arnold, P. Avouris, Z. W. Pan, Z. L. Wang. J. Phys. Chem. B 107, 659 (2003).
- 34. W. I. Park, J. S. Kim, G.-C. Yi, M. H. Bae, H.-J. Lee. Appl. Phys. Lett. 85, 5052 (2004).
- 35. P.-C. Chang, J. G. Lu. *IEEE Trans. Electron Devices* **55**, 2977 (2008).
- 36. S. Ju, K. Lee, M. H. Yoon, A. Facchetti, T. J. Marks, D. B. Janes. *Nanotechnology* **18**, 155201 (2007).
- 37. J. Guo, J. Wang, E. Polizzi, S. Datta, M. Lundstrom. IEEE Trans. Nanotechnol. 2, 329 (2003).

- 38. Y. C. Yeo. Thin Solid Films 462-463, 34 (2004).
- 39. G. Eranna, B. C. Joshi, D. P. Runthala, R. P. Gupta. Crit. Rev. Solid State Mater. Sci. 29, 111 (2004).
- 40. F. M. Hossain, J. Nishii, S. Takagi, A. Ohtomo, T. Fukumura, H. Fujioka, H. Ohno, H. Koinuma, M. J. Kawasaki. *Appl. Phys.* **94**, 7768 (2003).
- 41. Y. Yoon, J. Lin, S. J. Pearton, J. Guo. J. Appl. Phys. 101, 024301 (2007).
- 42. Z.-M. Liao, K.-J. Liu, J.-M. Zhang, J. Xu, D.-P. Yu. Phys. Lett. A 367, 207 (2007).
- 43. F. Jones, F. Léonard, A. A. Talin, N. S. Bell. J. Appl. Phys. 102, 014305 (2007).
- 44. E. M. Kaidashev, M. Lorenz, H. Wenckstern, A. Rahm, H. C. Semmelhack, K. H. Han, G. Benndorf, C. Bundrsmann, H. Hochmuth, M. Grundmann. *Appl. Phy. Lett.* **82**, 3901 (2003).
- 45. S. H. Jo, J. Y. Lao, Z. F. Ren, R. A. Farrer, T. Baldacchini, J. T. Fourkas. *Appl. Phys. Lett.* **83**, 4821 (2003).
- 46. K. J. Kang, C. Yoon, D. Y. Jeong, B. M. Moon, S. Kim. Jpn. J. Appl. Phys. 46, 6230 (2007).
- C. Bekeny, T. Voss, B. Hilker, J. Gutowski, R. Hauschild, H. Kalt, B. Postels, A. Bakin, A. Waag. J. Appl. Phys. 102, 044908 (2007).
- 48. G. Jo, W.-K. Hong, J. Maeng, M. Choe, W. Park, T. Lee. Appl. Phys. Lett. 94, 173118 (2009).
- 49. A. B. Djurišić, Y. H. Leung. Small 2, 944 (2006).
- 50. R.-C. Wang, C.-P. Liu, J.-L. Huang, S.-J. Chen. Appl. Phys. Lett. 87, 053103 (2005).
- 51. L. E. Greene, M. Law, J. Goldberger, F. Kim, J. C. Johnson, Y. Zhang, R. J. Saykally, P. Yang. *Angew. Chem.*, *Int. Ed.* 42, 3031 (2003).
- 52. H. J. Fan, R. Scholz, F. M. Kolb, M. Zacharias. Appl. Phys. Lett. 85, 4142 (2004).
- 53. H. J. Fan, R. Scholz, F. M. Kolb, M. Zacharias, U. Gcsele, F. Heyroth, C. Hempel, T. Eisenschmidt, J. Christen. *Appl. Phys. A* **79**, 1895 (2004).
- 54. X. Q. Meng, D. Z. Shen, J. Y. Zhang, D. X. Zhao, Y. M. Lu, L. Dong, Z. Z. Zhang, Y. C. Liu, X. W. Fan. *Solid State Commun.* **135**, 179 (2005).
- 55. L. Wang, X. Zhang, S. Zhao, G. Zhou, Y. Zhou, J. Qi. Appl. Phys. Lett. 86, 024108 (2005).
- H. T. Ng, B. Chen, J. Li, J. Han, M. Meyyappan, J. Wu, S. X. Li, E. E. Haller. *Appl. Phys. Lett.* 82, 2023 (2003).
- 57. D. Zhao, C. Andreazza, P. Andreazza, J. Ma, Y. Liu, D. Shen. Chem. Phys. Lett. 399, 522 (2004).
- 58. L. Huang, S. Wright, S. Yang, D. Shen, B. Gu, Y. Du. J. Phys. Chem. B 108, 19901 (2004).
- 59. F. Wen, W. Li, J.-H. Moon, J.-H. Kim. Solid State Commun. 135, 34 (2005).
- 60. Q. Yang, K. Tang, J. Zuo, Y. Qian. Appl. Phys. A 79, 1847 (2004).
- 61. F. Wang, Z. Ye, D. Ma, L. Zhu, F. Zhuge. J. Cryst. Growth 274, 447 (2005).
- 62. S. Choopun, N. Hongsith, S. Tanunchai, T. Chairuangsri, C. Krua-in, S. Singkarat, T. Vilathong, P. Mangkorntong, N. Mangkorntong. *J. Cryst. Growth* **282**, 365 (2005).
- 63. W. Yu, X. Li, X. Gao. Cryst. Growth Des. 5, 151 (2005).
- 64. W. Gcpel, U. Lampe. Phys. Rev. B 22, 6447 (1980).
- 65. S. Hong, T. Joo, W. I. Park, Y. H. Jun, G.-C. Yi. Appl. Phys. Lett. 83, 4157 (2003).
- 66. Y. Gu, I. Kuskovsky, M. Yin, S. O'Brien, G. F. Neumark. Appl. Phys. Lett. 85, 3833 (2004).
- 67. T. B. Hur, Y.-H. Hwang, H.-K. Kim. Appl. Phys. Lett. 86, 193113 (2005).
- 68. Y.-Y. Peng, T.-E. Hsieh, C.-H. Hsu. Appl. Phys. Lett. 89, 211909 (2006).
- 69. X. Wang, Y. Ding, C. J. Summers, Z. L. Wang. J. Phys. Chem. B 108, 8773 (2004).
- 70. J. Han, P. Q. Mantas, A. M. R. Senos. J. Eur. Ceram. Soc. 22, 49 (2002).
- 71. L. Schmidt-Mende, J. L. MacManus-Driscoll. Mater. Today 10, 40 (2007).
- 72. M. H. Huang, S. Mao, H. Feick, H. Yan, Y. Wu, H. Kind, E. Weber, R. Russo, P. Yang. *Science* **292**, 1897 (2001).
- 73. Y. Q. Chen, J. Jiang, Z. Y. He, Y. Su, D. Cai, L. Chen. Mater. Lett. 59, 3280 (2005).
- 74. S. M. Abrarov, Sh. U. Yuldashev, T. W. Kim, S. B. Lee, Y. H. Kwon, T. W. Kang. *Opt. Commun.* **250**, 111 (2005).
- 75. X. Liu, X. Wu, H. Cao, R. P. H. Chang. J. Appl. Phys. 95, 3141 (2004).

- Z. Chen, N. Wu, Z. Shan, M. Zhao, S. Li, C. B. Jiang, M. K. Chyu, S. X. Mao. Scr. Mater. 52, 63 (2005).
- 77. D. C. Reynolds, D. C. Look, B. Jogai. J. Appl. Phys. 89, 6189 (2001).
- 78. A. van Dijken, E. Meulenkamp, D. Vanmaekelbergh, A. Meijerink. *J. Phys. Chem. B* **104**, 1715 (2000).
- 79. A. van Dijken, E. Meulenkamp, D. Vanmaekelbergh, A. Meijerink. J. Lumin. 90, 123 (2000).
- 80. Y. W. Heo, D. P. Norton, S. J. Pearton. J. Appl. Phys. 98, 073502 (2005).
- 81. Q. X. Zhao, P. Klason, M. Willander, H. M. Zhong, W. Lu, J. H. Yang. *Appl. Phys. Lett.* **87**, 211912 (2005).
- 82. A. B. Djurišić, W. C. H. Choy, V. A. L. Roy, Y. H. Leung, C. Y. Kwong, K. W. Cheah, T. K. Gundu Rao, W. K. Chan, H. F. Lui, C. Surya. *Adv. Funct. Mater.* **14**, 856 (2004).
- 83. N. E. Hsu, W. K. Hung, Y. F. Chen. J. Appl. Phys. 96, 4671 (2004).
- 84. M. H. Huang, Y. Wu, H. Feick, N. Tran, E. Weber, P. Yang. Adv. Mater. 13, 113 (2001).
- 85. D. Li, Y. H. Leung, A. B. Djurišić, Z. T. Liu, M. H. Xie, S. L. Shi, S. J. Xu, W. K. Chan. *Appl. Phys. Lett.* **85**, 1601 (2004).
- 86. C. Hsu, Y. Lin, S. Chang, T. Lin, S. Tsai, I. Chen. Chem. Phys. Lett. 411, 221 (2005).
- 87. S. Z. Li, C. L. Gan, H. Cai, C. L. Yuan, J. Guo, P. S. Lee, J. Ma. *Appl. Phys. Lett.* **90**, 263106 (2007).
- 88. W. I. Park, J. Yoo, D. W. Kim, G. C. Yi, M. Kim. J. Phys. Chem. B 110, 1516 (2006).
- 89. Y. H. Park, Y. H. Shin, S. J. Noh, Y. Kim, S. S. Lee, C. G. Kim, K. S. An, C. Y. Park. *Appl. Phys. Lett.* **91**, 012102 (2007).
- 90. J. P. Richters, T. Voss, D. S. Kim, R. Scholz, M. Zacharias. Nanotechnology 19, 305202 (2008).
- 91. L. Yu, X.-F. Yu, Y. Qiu, Y. Chen, S. Yang. Chem. Phys. Lett. 465, 272 (2008).
- 92. V. V. Travnikov, A. Freiberg, S. F. Savikhin. J. Lumin. 47, 107 (1990).
- 93. T. Voss, L. Wischmeier. J. Nanosci. Nanotechnol. 8, 228 (2008).
- 94. L. Wischmeier, T. Voss, S. Börner, W. Schade. Appl. Phys. A 84, 111 (2006).
- 95. Y. Yang, B. K. Tay, X. W. Sun, J. Y. Sze, Z. J. Han, J. X. Wang, X. H. Zhang, Y. B. Li, S. Zhang. *Appl. Phys. Lett.* **91**, 071921 (2007).
- 96. J. Grabowska, A. Meany, K. K. Nanda, J.-P. Mosnier, M. O. Henry, J.-R. Duclère, E. McGlynn. *Phys. Rev. B* **71**, 115439 (2005).
- 97. J. Fallert, R. Hauschild, F. Stelzl, A. Urban, M. Wissinger, H. Zhou, C. Klingshim, H. Kalt. J. Appl. Phys. 101, 073506 (2007).
- 98. J. H. He, P. H. Chang, C. Y. Chen, K. D. Tsai. Nanotechnology 20, 135701 (2009).
- 99. K. Keem, H. Kim, G.-T. Kim, J. S. Lee, B. Min, K. Cho, M.-Y. Sung, S. Kim. *Appl. Phys. Lett.* **84**, 4376 (2004).
- C. S. Lao, M. C. Park, Q. Kuang, Y. L. Deng, A. K. Sood, D. L. Polla, Z. L. Wang. J. Am. Chem. Soc. 129, 12096 (2007).
- J. H. He, Y. H. Lin, M. E. McConney, V. V. Tsukruk, Z. L. Wang, G. Bao. J. Appl. Phys. 102, 084303 (2007).
- 102. D. Lin, H. Wu, W. Zhang, H. Li, W. Pan. Appl. Phys. Lett. 94, 172103 (2009).
- J. Zhou, Y. Gu, Y. Hu, W. Mai, P. H. Yeh, G. Bao, A. K. Sood, D. L. Polla, Z. L. Wang. *Appl. Phys. Lett.* 94, 191103 (2009).
- 104. R. K. Joshi, Q. Hu, F. Am, N. Joshi, A. Kumar. J. Phys. Chem. C 113, 16199 (2009).
- 105. T. J. Hsueh, Y. W. Chen, S. J. Chang, S. F. Wang, C. L. Hsu, Y. R. Lin, T. S. Lin, I. C. Chen. *J. Electrochem. Soc.* **154**, J393 (2007).
- 106. L. Liao, H. B. Lu, J. C. Li, C. Liu, D. J. Fu, Y. L. Liu. Appl. Phys. Lett. 91, 173110 (2007).
- 107. J. H. He, C. H. Ho, C. Y. Chen. Nanotechnology 20, 065503 (2009).
- 108. F. Zhiyong, J. G. Lu. In *Sensors*, 2005 IEEE, pp. 834–836 (2005).
- 109. E. Comini, C. Baratto, G. Faglia, M. Ferroni, G. Sberveglieri. J. Phys. D 40, 7255 (2007).
- 110. D. Kohl. In Elsevier Science SA, Lausanne, pp. 158-165 (1990).

- 111. Q. H. Li, Y. X. Liang, Q. Wan, T. H. Wang. Appl. Phys. Lett. 85, 6389 (2004).
- 112. Z. Y. Fan, D. W. Wang, P. C. Chang, W. Y. Tseng, J. G. Lu. Appl. Phys. Lett. 85, 5923 (2004).
- 113. C. Y. Lu, S. P. Chang, S. J. Chang, T. J. Hsueh, C. L. Hsu, Y. Z. Chiou, C. Chen. *IEEE Sens. J.* **9**, 485 (2009).
- 114. E. Comini, G. Faglia, G. Sberveglieri, Z. W. Pan, Z. L. Wang. Appl. Phys. Lett. 81, 1869 (2002).
- 115. G. Kwak, K. J. Yong. J. Phys. Chem. C 112, 3036 (2008).
- 116. L. Liao, H. B. Lu, J. C. Li, H. He, D. F. Wang, D. J. Fu, C. Liu. *J. Phys. Chem. C* 111, 1900 (2007).
- 117. C. C. Li, Z. F. Du, L. M. Li, H. C. Yu, Q. Wan, T. H. Wang. Appl. Phys. Lett. 91, 032101 (2007).
- 118. Z. Y. Fan, J. G. Lu. Appl. Phys. Lett. 86, 123510 (2005).
- 119. C. C. Li, L. M. Li, Z. F. Du, H. C. Yu, Y. Y. Xiang, Y. Li, Y. Cai, T. H. Wang. *Nanotechnology* **19**, 035501 (2008).
- 120. J. B. K. Law, J. T. L. Thong. Nanotechnology 19, 205502 (2008).
- 121. T. Y. Wei, P. H. Yeh, S. Y. Lu, Z. L. Wang. J. Am. Chem. Soc. 131, 17690 (2009).
- 122. S. J. Chang, T. J. Hsueh, I. C. Chen, B. R. Huang. Nanotechnology 19, 175502 (2008).
- 123. E. Wongrat, P. Pimpang, S. Choopun. Appl. Surf. Sci. 256, 968 (2009).
- 124. Y. Zhang, Q. Xiang, J. Q. Xu, P. C. Xu, Q. Y. Pan, F. Li. J. Mater. Chem. 19, 4701 (2009).
- 125. Y. Zeng, T. Zhang, L. J. Wang, M. H. Kang, H. T. Fan, R. Wang, Y. He. *Sens. Actuators, B* **140**, 73 (2009).
- 126. N. Kakati, S. H. Jee, S. H. Kim, H. K. Lee, Y. S. Yoon. Jpn. J. Appl. Phys. 48, 105002 (2009).
- 127. B. O'Regan, M. Grätzel. Nature 353, 737 (1991).
- 128. K. Y. Cheung, C. T. Yip, A. B. Djurišić, Y. H. Leung, W. K. Chan. *Adv. Funct. Mater.* 17, 555 (2007).
- 129. K. Sayama, H. Suguhara, H. Arakawa. Chem. Mater. 10, 3825 (1998).
- 130. M. D. Archer, A. J. Nozik. *Nanostructured and Photoelectrochemical Systems for Solar Photon Conversion*, World Scientific (2008).
- 131. E. Galoppini, J. Rochford, H. H. Chen, G. Saraf, T. C. Lu, A. Hagfeldt, G. Boschloo. *J. Phys. Chem. B* **110**, 16159 (2006).
- 132. E. A. Meulenkamp. J. Phys. Chem. B 103, 7831 (1999).
- 133. D. C. Look, D. C. Reynolds, J. R. Sizelove, R. L. Jones, C. W. Litton, G. Cantwell, W. C. Harsch. *Solid State Commun.* **105**, 399 (1998).
- 134. Y. S. Yun, J. Y. Park, H. Oh, J. J. Kim, S. S. Kim. J. Mater. Res. 21, 132 (2006).
- 135. M. Saito, S. Fujihara. Energy Environ. Sci. 1, 280 (2008).
- 136. Y. Zhang, L. Wu, Y. Liu, E. Xie. J. Phys. D 42, 085105 (2009).
- 137. V. Dhas, S. Muduli, W. Lee, S. H. Han, S. Ogale. Appl. Phys. Lett. 93, 243108 (2008).
- 138. K. Keis, J. Lindgren, S. E. Lindquist, A. Hagfeldt. Langmuir 16, 4688 (2000).
- 139. M. Law, L. E. Greene, A. Radenovic, T. Kuykendall, J. Liphardt, P. Yang. *J. Phys. Chem. B* **110**, 22652 (2006).
- 140. M. Wang, C. Huang, Y. Cao, Q. Yu, W. Guo, Q. Huang, Y. Liu, J. Huang, H. Wang, Z. Deng. *Appl. Phys. Lett.* **94**, 263506 (2009).
- M. Wang, C. Huang, Y. Cao, Q. Yu, Z. Deng, Y. Liu, Z. Huang, J. Huang, Q. Huang, W. Guo, J. Liang. J. Phys. D 42, 155104 (2009).
- 142. F. A. Kroger. *The Chemistry of Imperfect Crystals*, 2nd ed., North Holland (1974).
- 143. G. Redmond, D. Fitzmauricem, M. Grätzel. Chem. Mater. 6, 686 (1994).
- 144. A. R. Rao, V. Dutta. Nanotechnology 19, 445712 (2008).
- 145. Z. L. S. Seow, A. S. W. Wong, V. Thavasi, R. Jose, S. Ramakrishna, G. W. Ho. *Nanotechnology* **20**, 045604 (2009).
- 146. W. Zhang, R. Zhu, X. Liu, B. Liu, S. Ramakrishna. Appl. Phys. Lett. 95, 043304 (2009).
- 147. D. I. Suh, S. Y. Lee, T. H. Kim, J. M. Chun, E. K. Suh, O. B. Yang, S. K. Lee. *Chem. Phys. Lett.* **442**, 348 (2007).

- 148. M. S. Akhtar, M. A. Khan, M. S. Jeon, O. B. Yang. *Electrochim. Acta* 53, 7869 (2008).
- 149. Y. F. Hsu, Y. Y. Xi, C. T. Yip, A. B. Djurišić, W. K. Chan. J. Appl. Phys. 103, 083114 (2008).
- 150. W. Chen, H. Zhang, I. M. Hsing, S. Yang. *Electrochem. Commun.* 11, 1057 (2009).
- 151. A. E. Suliman, Y. T. Tang, L. Xu. Solar Energy Mater. Solar Cells 91, 1658 (2007).
- 152. T. W. Hamann, A. B. F. Martinson, J. W. Elam. Adv. Mater. 20, 1560 (2008).
- 153. Q. Zhang, T. P. Chou, B. Russo, S. A. Jenekhe, G. Cao. Angew. Chem., Int. Ed. 47, 2402 (2008).
- 154. I. D. Kim, J. M. Hong, B. H. Lee, D. Y. Kim, E. K. Jeon, D. K. Choi, D. J. Yang. *Appl. Phys. Lett.* **91**, 163109 (2007).
- 155. T. P. Chou, Q. Zhang, G. E. Fryxell, G. Cao. Adv. Mater. 19, 2588 (2007).